










RESEARCH ARTICLE | NOVEMBER 25 2024

Internal quantum efficiency of GaAsBi MQW structure for the active region of VECSELs

Special Collection: [Defects in Solids for Quantum Technologies](#)

A. Štaupienė ; A. Zelioli ; A. Špokas ; A. Vaitkevičius ; B. Čechavičius ; S. Stanionytė ; S. Raišys ; R. Butkutė ; E. Dudutienė 

 Check for updates

Appl. Phys. Lett. 125, 221102 (2024)

<https://doi.org/10.1063/5.0234853>



Articles You May Be Interested In

KoopmanLab: Machine learning for solving complex physics equations

APL Mach. Learn. (September 2023)

Experimental realization of a quantum classification: Bell state measurement via machine learning

APL Mach. Learn. (September 2023)

Internal quantum efficiency of GaAsBi MQW structure for the active region of VECSELs

Cite as: Appl. Phys. Lett. **125**, 221102 (2024); doi: [10.1063/5.0234853](https://doi.org/10.1063/5.0234853)

Submitted: 23 August 2024 · Accepted: 9 November 2024 ·

Published Online: 25 November 2024



View Online



Export Citation



CrossMark

A. Štaupienė,^{1,2,a)} A. Zelioli,¹ A. Špokas,^{1,2} A. Vaitkevičius,^{1,2} B. Čechavičius,¹ S. Stanionytė,¹ S. Raišys,² R. Butkutė,¹ and E. Dudutienė¹

AFFILIATIONS

¹Center for Physical Sciences and Technology, Saulėtekio av. 3, LT-10257 Vilnius, Lithuania

²Faculty of Physics, Vilnius University, Saulėtekio av. 3, LT-10257 Vilnius, Lithuania

Note: This paper is part of the Special Topic, Defects in Solids for Quantum Technologies.

^{a)}Author to whom correspondence should be addressed: aiste.staupiene@ftmc.lt

ABSTRACT

We present a detailed study on the optical properties of GaAsBi/GaAs multiple quantum well structure, optimized for the active area for vertical-external-cavity surface-emitting lasers. The quantum structure was grown by molecular beam epitaxy with every other barrier made thinner to have a homogeneous structure with high photoluminescence (PL) intensity. PL measurements were carried out in a wide temperature range from 4 to 300 K. The PL band of 1.085 eV was attributed to the optical transition in QWs with 8.0%Bi. The S-shaped temperature dependence of PL peak positions showed high localization effect of 30 meV. The internal quantum efficiency (IQE) was evaluated for the bismide structures with a modified ABB* method, which includes contribution from trap-assisted Auger recombination. The calculations showed low IQE of <0.025% for GaAs_{0.92}Bi_{0.08}/GaAs 12 QWs structure, which was explained by the low growth temperature, resulting in a high density of point defects in the material.

© 2024 Author(s). All article content, except where otherwise noted, is licensed under a Creative Commons Attribution (CC BY) license (<https://creativecommons.org/licenses/by/4.0/>). <https://doi.org/10.1063/5.0234853>

Vertical-external-cavity surface-emitting lasers (VECSELs) are highly versatile semiconductor lasers renowned for their tunability, efficiency, high beam quality, and power scalability, providing output powers ranging from milliwatts to tens of watts, which is beneficial for both low- and high-power applications.¹ The VECSEL gain chip is structurally composed of a highly reflective mirror and a semiconductor gain region. The latter typically includes multiple quantum well (MQW) layers separated by barrier layers. The high gain is achieved by placing the quantum wells (QWs) periodically at the antinodes of the optical standing wave. InGaAs/GaAs QWs are typically used for the gain region of VECSELs emitting in the wavelength range of 920–1100 nm.^{2–3} However, it is challenging to reach emission at longer wavelengths due to increased strain in InGaAs QWs. Therefore, we present bismuth-containing compounds as a potential material for the active area in such emitters. With an increase in Bi content, the bandgap of GaAsBi significantly shifts to lower energies of approximately 60–90 meV per %Bi.⁴ Moreover, the incorporation of Bi also induces strong spin-orbit splitting, surpassing the bandgap energy when Bi content exceeds 10.5%.⁵ This can have beneficial effect of suppressing Auger recombination and inter-valence band absorption processes.

Additionally, the bandgap of GaAsBi has low sensitivity to temperature variations.⁶ This makes GaAsBi QW structures a promising active medium for stable room temperature operations of optoelectronic devices such as VECSELs. However, the growth of GaAsBi quantum structures is challenging, as it requires low growth temperatures and stoichiometric As₂/Ga flux ratios in order to incorporate large Bi atoms into the GaAs lattice.⁷ This leads to a high point defect density, resulting in a significant reduction in GaAsBi luminescence intensity and emission efficiency.⁸ Therefore, optimizing the growth conditions to enhance the quality of GaAsBi is crucial for developing efficient near-infrared (NIR) sources, necessitating the study of its optical properties. For this reason, a detailed optical study using photoluminescence (PL) technique was conducted to investigate optical characteristics, especially the internal quantum efficiency (IQE), of a GaAsBi/GaAs multiple quantum well structures. We calculated photoluminescence emission efficiency, analyzed different carrier recombination processes, and demonstrated methods to quantitatively evaluate the QW photoluminescence efficiency for bismide structures. The investigation of IQE for all GaAsBi/GaAs QW structures allows not only to compare structures grown, characterized in different laboratories, but also to evaluate the

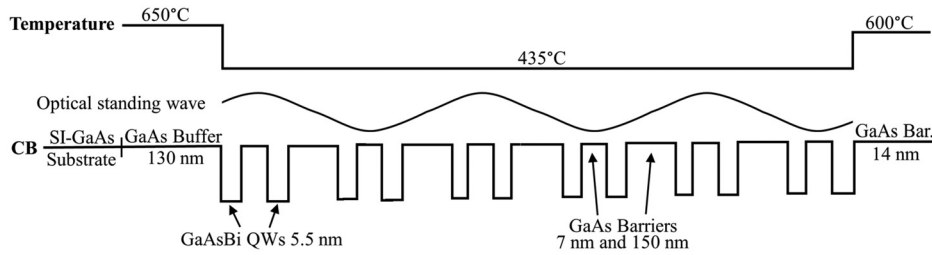


FIG. 1. Growth protocol [temperature profile (top picture) and conduction band sketch (bottom picture)] of GaAsBi/GaAs MQW structure (sample 1) as an active area for VECSEL with six pairs of GaAsBi QWs with a width of 5.5 nm and alternating GaAs barriers of 7 and 150 nm. Thicknesses are not to scale.

amount of non-radiative recombination, which can enhance the optimization of GaAsBi structure growth.

Our studied structures were grown by the molecular beam epitaxy (MBE) method using Veeco GENxplor R&D MBE system, equipped with metallic Ga, Bi sources, and a two-zone valved cracker source, providing a purely dimeric arsenic (As_2) flux and an ability to finely tune the beam pressure. Epitaxial layers were deposited on the semi-insulating GaAs (100) substrate ($350 \mu\text{m}$). GaAs buffer layer was grown at 650°C to ensure high surface smoothness, while GaAs barriers and GaAsBi QWs were grown at 435 and 425°C , respectively, for the active area for VECSEL (sample 1) and its reference (sample 2). Here, the temperature values were recorded via a thermocouple mounted in-between the substrate heater and the sample. However, due to the position, the thermocouple overestimates the real substrate temperature during the growth.

The first structure consisted of 12 QWs with a width of 5.5 nm, while barrier widths were set alternating to 7 and 150 nm (see Fig. 1). This structure represents a design for the active area for VECSELs and was designed such that the antinodes of the standing wave would align with the thin barrier in between a couple of QWs. The QW thickness is fixed to achieve a specific emission energy, while the thin barrier thickness needs to be thick enough for the QWs to be confined and as thin as possible to lower the overall thickness of the gain region, for this reason 7 nm was chosen. To achieve the desired wave alignment, the optical thickness of the thin barrier, combined with the QW and the thick barrier, must equal half of the target emission wavelength. By imposing this constraint, the necessary thickness for the thick barrier was calculated. Advantages of this optimized design include more compact gain region, increased homogeneity, and enhanced PL intensities.⁹ The second structure contained 12 QWs with a width of 5.5 nm as well, while barrier widths were 7 nm. This structure was selected as a reference sample for the first structure, due to the same QW parameters and emission energy. Structures contained 8.0%Bi and 7.6%Bi, respectively, for structures 1 and 2, which was determined by X-ray diffraction (XRD).

Temperature-dependent photoluminescence (TDPL) measurement was conducted in a variable-temperature (4–300 K) closed-cycle He cryostat. Photoluminescence measurements were performed using 532 nm central wavelength excitation from diode pumped solid state (DPSS) laser with maximum output power of 400 mW. The excitation power was varied from 0.5 to 330 mW using neutral density filters. A focusing lens ($f = 150 \text{ mm}$) was used to focus the laser beam into a $\sim 0.02 \text{ mm}^2$ spot on the sample surface. The luminescence was detected by a liquid nitrogen-cooled InGaAs photodetector using a lock-in amplification technique.

TDPL measurement was conducted for sample 1 using 14 mW excitation in a wide temperature range of 4–300 K. The TDPL spectra are presented in Fig. 2.

The PL band of 1.085 eV at 300 K was assigned to optical transitions in GaAsBi QWs. Also, the appearance of red-blue-red shift (S-shape) in the PL peak position dependence on temperature can be observed, which indicates carrier localization [see Fig. 3(a)].

This typical S-shape behavior can be explained by localized states caused by alloy disorder, defects or strain introduced by bismuth incorporation.¹⁰ The initial red-blue shift of the PL peak position accounts for the carrier transport between deep and shallow localization centers, while the second redshift at high temperatures is due to bandgap narrowing with temperature.¹¹

The blueshift rate of the bandgap as a function of temperature and carrier localization can be evaluated by fitting the photoluminescence peak position dependence on temperature with Varshni–Eliseev function,¹²

$$E_g = E_0 - \frac{\alpha T^2}{\beta + T} - \frac{\sigma^2}{k_B T}. \quad (1)$$

Here, E_g is the bandgap energy, E_0 is the bandgap energy at 0 K temperature, α —Varshni parameter that indicates how rapidly the bandgap energy changes with temperature, β is Varshni parameter, which is related to the Debye temperature and was fixed at 204 K,¹³ and σ is the Eliseev parameter, which represents the dispersion of localized states with a Gaussian distribution.¹⁴ The obtained fitting

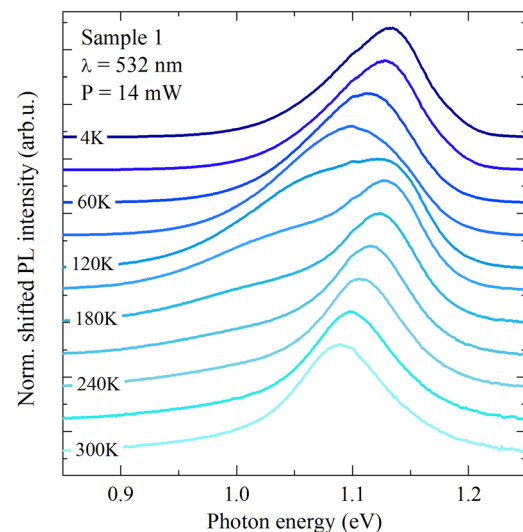


FIG. 2. TDPL spectra of GaAsBi/GaAs structure (sample 1). The spectra are normalized and shifted for better visualization.

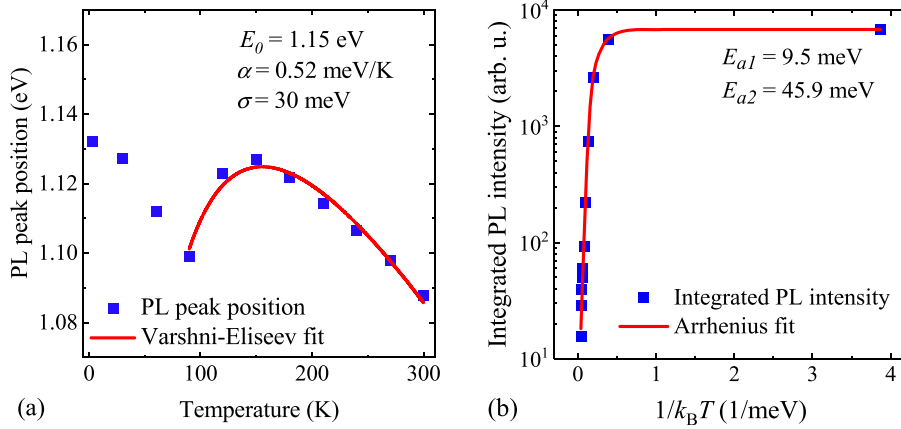


FIG. 3. (a) PL peak position dependence on the temperature. Symbols correspond to the experimental data; the solid line is fitted using the Varshni-Eliseev equation (1). (b) Integrated PL intensity dependence on the temperature. Symbols correspond to the experimental data; the solid line is fitted using the Arrhenius equation (2).

parameters showed that $E_0 = 1.15 \pm 0.01$ eV, $\alpha = 0.52 \pm 0.03$ meV/K, and $\sigma = 30 \pm 2$ meV. The dispersion of Gaussian density of localized states for carriers (σ parameter) indicates that structure has high localization effect, which is present even at room temperature.

Integrated PL intensity dependence on the temperature is demonstrated in Fig. 3(b). PL thermal quenching process was fitted with modified Arrhenius equation¹⁵ with two activation energies,

$$I(T) = \frac{I_0}{1 + a_1 \exp\left(-\frac{E_{a1}}{k_B T}\right) + a_2 \exp\left(-\frac{E_{a2}}{k_B T}\right)}. \quad (2)$$

Here, I_0 is the integrated PL intensity at 4 K, and a_1 and a_2 are fitting coefficients related to the activation energies E_{a1} and E_{a2} . Lower activation energy $E_{a1} = 9.5 \pm 0.1$ meV can be attributed to the non-radiative recombination due to Bi pairs and clusters, while the higher activation energy $E_{a2} = 45.9 \pm 1.1$ meV can be assigned to the inhomogeneity of the structure.¹¹

The absolute internal quantum efficiency measurement was performed for both samples using a different setup with an Edinburg Instruments integrating sphere and an 830 nm central wavelength continuous-wave CW laser with maximum output power of 132 mW as an excitation source. The spectrometer used in this setup is an Andor Kymera 328i, which is used in combination with an iDUS 1.7 μ m InGaAs detector.

IQE efficiency was evaluated using a two-measurement approach, which requires a measurement without the sample in the sphere and a measurement where the sample is in the sphere and in the path of the laser beam.¹⁶ Using this approach, the IQE is calculated using the following equation:¹⁷

$$IQE = \frac{P_c}{L_a - L_c}. \quad (3)$$

Here, P_c is the number of photons in the wavelength region of the emission, and L_a and L_c are the number of photons in the wavelength region of the excitation. The measurement results are shown in Fig. 4.

This method gave IQE values of 0.010% and 0.013% for structures 1 and 2, respectively. It should be noted that extremely low efficiency can be explained by the high levels of non-radiative recombination caused by the low growth temperature of the material, alloy disorder, and strain introduced by bismuth incorporation,

resulting in a high density of defects in the material.^{10,18} A higher efficiency of sample 2 can be explained by a lower Bi content and overall reduced barrier thickness. Moreover, the IQE value should depend on the number of QWs since it affects carrier confinement, recombination rates, and likelihood of defects, with an optimal number of QWs maximizing the IQE before non-radiative losses increases. Also, efficiency should decrease with increasing concentration of Bi, because it increases the disorder in GaAs lattice.

While the absolute IQE measurement with an integrating sphere is considered to be the most reliable, this method cannot give any additional information about the structure, such as the ratio between different carrier recombination mechanisms or the IQE dependence on the carrier concentration. As a result, alternative relative methods have been investigated.

The ABC model¹⁹ for IQE calculations employs room temperature photoluminescence measurements as a function of excitation power. This method includes contributions from three carrier recombination mechanisms: non-radiative recombination (An), radiative recombination (Bn^2), and Auger non-radiative recombination (Cn^3). Here, the IQE can be calculated using the following equation:

$$IQE = \frac{Bn^2}{An + Bn^2 + Cn^3} = \frac{Bn^2}{G}, \quad (4)$$

where generation rate G can be expressed in terms of integrated PL intensity I_{PL} ,

$$G = \frac{A\sqrt{I_{PL}}}{\sqrt{B\eta}} + \frac{I_{PL}}{\eta} + \frac{C\sqrt{(I_{PL})^3}}{\sqrt{(B\eta)^3}}, \quad (5)$$

where $I_{PL} = \eta Bn^2$, n is the carrier concentration, and η is a constant that incorporates PL collection efficiency and excitation volume. The generation rate can be separately expressed in terms of laser excitation power P_{laser} ,

$$G = xP_{laser}. \quad (6)$$

Where $x = \frac{(1-R)\alpha}{A_{spot}hv}$, R is the Fresnel reflection at the sample surface, α is the absorption coefficient of the active region, A_{spot} is the area of the laser spot on the sample surface and hv is the photon energy of the excitation laser. When combined, Eqs. (5) and (6) give,

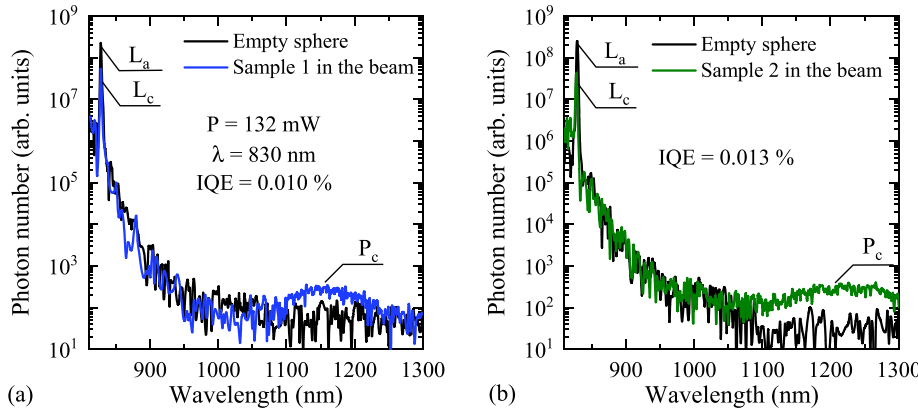


FIG. 4. Graphical representation of the absolute IQE measurement with an integrating sphere for (a) sample 1 and (b) sample 2. IQE was calculated using Eq. (3).

$$P_{\text{laser}} = \frac{A\sqrt{I_{\text{PL}}}}{x\sqrt{B\eta}} + \frac{I_{\text{PL}}}{x\eta} + \frac{C\sqrt{(I_{\text{PL}})^3}}{x\sqrt{(B\eta)^3}}. \quad (7)$$

By changing the terms $\frac{A}{x\sqrt{B\eta}}$, $\frac{1}{x\eta}$, and $\frac{C}{x\sqrt{(B\eta)^3}}$ into the fitting parameters P_1 , P_2 , and P_3 , respectively, IQE can be calculated as,²⁰

$$\text{IQE} = \frac{P_2 I_{\text{PL}}}{P_1 \sqrt{I_{\text{PL}}} + P_2 I_{\text{PL}} + P_3 I_{\text{PL}}^{3/2}} = \frac{I_{\text{PL}} P_2}{P_{\text{laser}}}. \quad (8)$$

Here, parameters P_1 (5.3 ± 0.6), P_2 (0.07 ± 0.01), and P_3 (1×10^{-17}) are obtained by fitting the integrated photoluminescence intensity measurement, for sample 1, as a function of excitation power, which is shown in Fig. 5(a). It can be seen that calculated IQE values are significantly larger compared to the absolute measurement results (Fig. 4), which indicates that an additional non-radiative recombination mechanism is needed and this ABC method should be modified.²¹

While the used fit [Fig. 5(a)] matches the dependency quite well ($R^2 = 0.996$), the values of parameters from ABC method cannot be adjusted to produce lower IQE values. Therefore, a new parameter, which lowers IQE and does not affect the dependency of the fit, should be added. The ABC+B' model was proposed by Espenlaub *et al.*²² This modified model is an improved ABC model with an additional non-radiative recombination mechanism — a trap-assisted hot carrier generation process. This method is designed for low efficiency structures grown at low temperatures. It is explained that trap-assisted recombination, such as trap-assisted Auger recombination (TAAR), has high impact on IQE of structures grown at low temperatures, due to the high concentration of defects, which act as non-radiative recombination centers. Moreover, as TAAR involves two carriers, this makes it a second order recombination mechanism (B^*n^2).²³ This non-radiative bimolecular term added to Eq. (4) decreases the IQE value without changing the shape or dependency of the fit.

Moreover, the fitting parameter P_3 , which corresponds to Auger non-radiative recombination, was negligible and did not give any contribution to the IQE value. Therefore, we changed the ABC method by eliminating the Auger non-radiative recombination (Cn^3) and adding trap-assisted Auger recombination (B^*n^2) channels. This resulted in modified IQE equations (9) and (10),

$$\text{IQE} = \frac{Bn^2}{An + Bn^2 + B^*n^2}, \quad (9)$$

$$\text{IQE} = \frac{P_2 I_{\text{PL}}}{P_1 \sqrt{I_{\text{PL}}} + P_2 I_{\text{PL}} + P_2^* I_{\text{PL}}} = \frac{I_{\text{PL}} P_2}{P_{\text{laser}}}. \quad (10)$$

By establishing the values of fitting parameters P_1 and $P_2 + P_2^*$ from Fig. 5(a) and IQE value from absolute measurement (Fig. 4), this modified ABB* method can be employed. By fitting the same integrated photoluminescence intensity dependence on excitation power with new generation rate equation,

$$G = P_1 \sqrt{I_{\text{PL}}} + P_2 I_{\text{PL}} + P_2^* I_{\text{PL}}, \quad (11)$$

parameters P_2 ($3.7 \times 10^{-5} \pm 4 \times 10^{-6}$) and P_2^* ($7.3 \times 10^{-2} \pm 1.2 \times 10^{-2}$) are obtained for sample 1. The same process is then repeated for sample 2 [Fig. 5(c)], and parameters P_1 (7.4 ± 0.1), P_2 ($7.0 \times 10^{-5} \pm 3 \times 10^{-6}$), and P_2^* ($8.0 \times 10^{-2} \pm 5 \times 10^{-3}$) are acquired. Trap-assisted Auger recombination parameter P_2^* is three orders of magnitude higher than radiative recombination parameter P_2 , which shows that TAAR has a great impact on the IQE of structures grown at such low temperatures.

Moreover, we can calculate the IQE values and analyze the ratio between different carrier recombination processes. Figure 5(b) shows the total non-radiative recombination efficiency and radiative recombination efficiency dependence on excitation power of sample 1. Here, the total non-radiative recombination efficiency is $\frac{P_1 \sqrt{I_{\text{PL}}} + P_2^* I_{\text{PL}}}{P_{\text{laser}}}$. It can be observed that the PL emission is dominated by non-radiative recombination and radiative recombination efficiency does not reach saturation, which means that higher excitation power conditions could be used to find the IQE saturation region.

While these fitting parameters P_1 , P_2 , and P_2^* can be determined without any knowledge about A , B , or B^* coefficients, they are arbitrary and do not hold any physical meaning. In order to calculate the value of carrier concentration or non-radiative coefficients, it is necessary to assume the value of radiative coefficient B , which is still unknown for the bismide structures.

It should be noted that all photoluminescence and IQE measurements were conducted using non-resonant excitation and there is a possibility that the photoexcited carriers in the GaAs barriers have

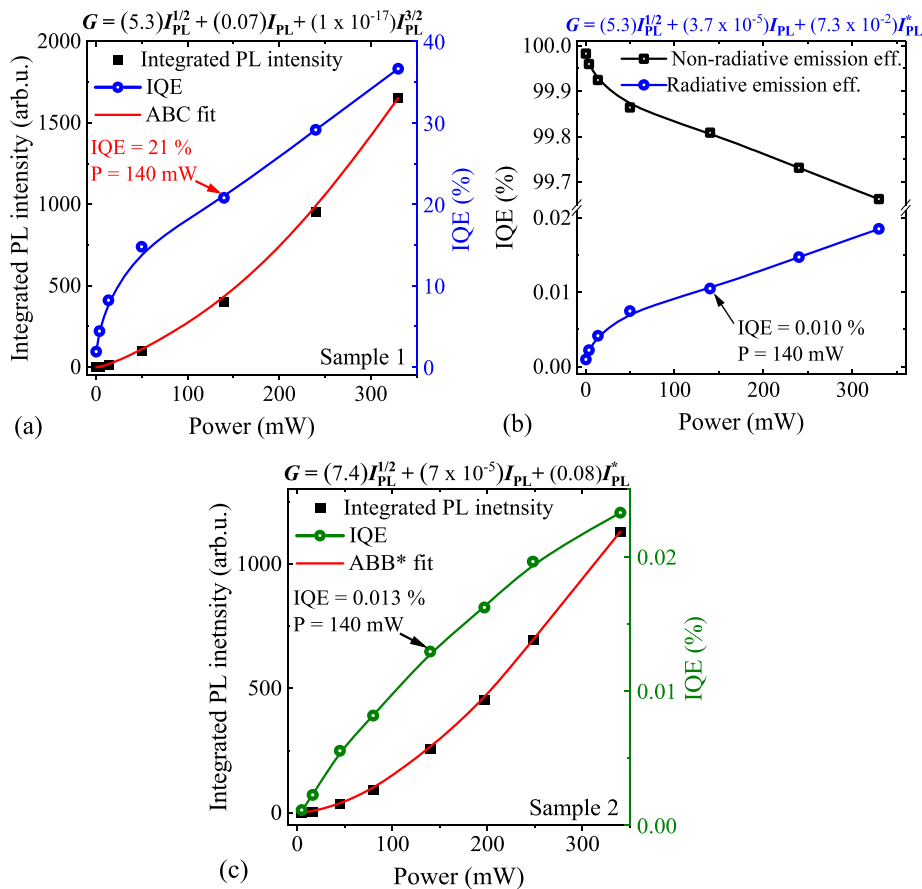


FIG. 5. (a) Graphical representation of the ABC method and calculated IQE values of sample 1. Black symbols correspond to the experimental data; the solid red line is fitted using Eq. (7); blue symbols correspond to calculated IQE values using Eq. (8). (b) Calculated emission efficiencies of sample 1 employing the ABB* method. Black symbols correspond to non-radiative emission efficiency; blue symbols correspond to calculated radiative emission efficiency using Eq. (10); and (c) Graphical representation of the ABB* method and calculated IQE values of sample 2. Black symbols correspond to the experimental data; the solid red line is fitted using Eq. (11); and green symbols correspond to calculated IQE values using Eq. (10).

contributed negatively to the PL intensity, thus resulting in the measured IQE being lower than is the actual case.

To conclude, we present detailed optical study on GaAsBi/GaAs MQW structure grown by MBE as a gain region for VECSELs. The PL band of 1.085 eV at 300 K was assigned to optical transitions in QWs of GaAsBi with 8%Bi. The TDPL measurements revealed S-shaped temperature dependence of PL peak positions, which was explained by the high localization effect of 30 meV, that is present even at room temperature.

Additionally, this study presents calculations of the emission efficiency of GaAsBi/GaAs MQW structures. We show a simple analysis method to not only calculate the IQE, but also the relative carrier recombination ratios. Our proposed modified ABB* method combines Yoo *et al.*²⁰ simplified relative ABC method and Espenlaub *et al.*²² extended ABC+B' model. We explain the use of additional non-radiative recombination mechanism by showing the difference between calculated IQE value (0.01% with 138 mW excitation) by the absolute method with an integrating sphere and the estimated IQE value (21% with 140 mW excitation) from the ABC method. Moreover, the elimination of the Auger non-radiative recombination mechanism is justified by the ABC model, where P_3 parameter was negligible and did not give any contribution to the IQE value. While this presented ABB* model cannot give absolute values of A , B , or B^* coefficients without any additional investigations, it can be utilized to

obtain the relative fitting parameters P_1 and $P_2 + P_2^*$ from power-dependent PL measurement and calculate the IQE dependency on excitation power of GaAsBi/GaAs MQW structures, without any assumptions about recombination coefficients.

See the [supplementary material](#) for the IQE calculation of the 2200 nm GaAsBi layer.

This work was supported by the Research Council of Lithuania under the Grant No. S-MIP-22-86.

AUTHOR DECLARATIONS

Conflict of Interest

The authors have no conflicts to disclose.

Author Contributions

A. Štaupienė: Formal analysis (lead); Investigation (equal); Methodology (equal); Visualization (lead); Writing – original draft (lead). **A. Zelioli:** Methodology (equal); Resources (equal); Writing – review & editing (equal). **A. Špokas:** Resources (equal); Writing – review & editing (equal). **A. Vaitkevičius:** Resources (equal); Writing – review & editing (equal). **B. Čechavičius:** Formal analysis (equal); Investigation (equal). **S. Stanionytė:** Formal analysis (equal);

Investigation (equal). **S. Raišys**: Formal analysis (equal); Investigation (equal). **R. Butkutė**: Project administration (lead); Resources (equal); Supervision (equal); Writing – review & editing (equal). **E. Dudutienė**: Conceptualization (lead); Methodology (equal); Supervision (equal); Writing – review & editing (equal).

DATA AVAILABILITY

The data that support the findings of this study are available within the article.

REFERENCES

- ¹M. Guina, A. Rantamäki, and A. Härkönen, *J. Phys. D* **50**, 383001 (2017).
- ²K. S. Kim, J. Yoo, G. Kim, S. Lee, S. Cho, J. Kim, T. Kim, and Y. Park, *IEEE Photonics Technol. Lett.* **19**(20), 1655–1657 (2007).
- ³K. S. Kim, J. R. Yoo, S. M. Lee, S. J. Lim, J. Y. Kim, J. H. Lee, S. H. Cho, T. Kim, and Y. J. Park, *J. Cryst. Growth* **287**(2), 629–632 (2006).
- ⁴M. Yoshimoto, S. Murata, A. Chayahara, Y. Horino, J. Saraie, and K. Oe, *Jpn. J. Appl. Phys., Part 1* **42**, L1235 (2003).
- ⁵Z. Batool, K. Hild, T. J. C. Hosea, X. Lu, T. Tiedje, and S. J. Sweeney, *J. Appl. Phys.* **111**(11), 113108 (2012).
- ⁶J. Yoshida, T. Kita, O. Wada, and K. Oe, *Jpn. J. Appl. Phys., Part 1* **42**, 371–374 (2003).
- ⁷S. Tixier, M. Adamczyk, T. Tiedje, S. Francoeur, A. Mascarenhas, P. Wei, and F. Schiettekatte, *Appl. Phys. Lett.* **82**(14), 2245–2247 (2003).
- ⁸B. Zhang, M. Jansson, P. P. Chen, X. J. Wang, W. M. Chen, and I. A. Buyanova, *Nanotechnology* **31**(22), 225706 (2020).
- ⁹A. Zelioli, A. Špokas, B. Čechavičius, M. Talaikis, S. Stanionytė, A. Vaitkevičius, A. Čerškus, E. Dudutienė, and R. Butkutė, *Sci. Rep.* (published online) (2024).
- ¹⁰L. Wang, L. Zhang, L. Yue, D. Liang, X. Chen, Y. Li, P. Lu, J. Shao, and S. Wang, *Crystals* **7**(3), 63 (2017).
- ¹¹T. Wilson, N. P. Hylton, Y. Harada, P. Pearce, D. Alonso-Álvarez, A. Mellor, R. D. Richards, J. P. R. David, and N. J. Ekins-Daukes, *Sci. Rep.* **8**, 6457 (2018).
- ¹²P. G. Eliseev, P. Perlin, J. Lee, and M. Osiński, *Appl. Phys. Lett.* **71**, 569 (1997).
- ¹³I. Vurgaftman, J. R. Meyer, and L. R. Ram-Mohan, *J. Appl. Phys.* **89**, 5815–5875 (2001).
- ¹⁴Y. P. Varshni, *Physica* **34**(1), 149–154 (1967).
- ¹⁵K. J. Laidler, *J. Chem. Educ.* **61**(6), 494–498 (1984).
- ¹⁶S. Leyre, E. Coutino-Gonzalez, J. J. Joos, J. Ryckaert, Y. Meuret, D. Poelman, P. F. Smet, G. Durinck, J. Hofkens, G. Deconinck, and P. Hanselaer, *Rev. Sci. Instrum.* **85**(12), 123115 (2014).
- ¹⁷H. Ishida, S. Tobita, Y. Hasegawa, R. Katoh, and K. Nozaki, *Coord. Chem. Rev.* **254**(21), 2449–2458 (2010).
- ¹⁸L. Gelczuk, J. Kopaczek, T. B. O. Rockett, R. D. Richards, and R. Kudrawiec, *Sci. Rep.* **7**, 12824 (2017).
- ¹⁹N. F. Mott, *Solid-State Electron.* **21**, 1275–1280 (1978).
- ²⁰Y. S. Yoo, T. M. Roh, J. H. Na, S. J. Son, and Y. H. Cho, *Appl. Phys. Lett.* **102**, 211107 (2013).
- ²¹K. Nomeika, Ž. Podlipskas, M. Nikitina, S. Nargelas, G. Tamulaitis, and R. Aleksiejūnas, *J. Mater. Chem. C* **10**, 1735–1745 (2022).
- ²²A. C. Espenlaub, D. J. Myers, E. C. Young, S. Marcinkevičius, C. Weisbuch, and J. S. Speck, *J. Appl. Phys.* **126**(18), 184502 (2019).
- ²³P. T. Landsberg and D. J. Robbins, *Solid State Electron.* **21**(11), 1289–1294 (1978).